

Surface-Temperature Measurement and Submicron Defect Isolation for Microelectronic Devices Using Thermoreflectance Microscopy

Seon Young Ryu · Dong Uk Kim · Jun Ki Kim · Hae Young Choi · Geon Hee Kim · Ki Soo Chang

Received: 15 November 2013 / Accepted: 30 June 2014 / Published online: 25 July 2014
© Springer Science+Business Media New York 2014

Abstract Thermal analysis of small defects becomes essential for understanding the influence of hotspots, which affect the device performance, such as the operating speed and reliability. In this paper, we demonstrate a CCD-based thermoreflectance microscopy (TRM) system as a noncontact thermal analysis technique especially for submicron defects on microelectronic devices. By employing a lock-in detection technique and temperature calibration process, the surface temperature distribution of a polysilicon microresistor and submicron defects that are not distinguishable in conventional optical microscope images can be quantitatively measured with high thermal (up to ~ 13 mK) and spatial (~ 670 nm) resolution. In addition, the accuracy of quantitative temperature measurement and small defect isolation by the TRM system is compared with that obtained from an infrared thermography (IRT) system.

Keywords Defect isolation · Temperature mapping · Thermoreflectance microscopy

1 Introduction

Failure detection during semiconductor fabrication is becoming even more important because small defects can cause various serious problems in microelectronic

Seon Young Ryu, Dong Uk Kim, and Jun Ki Kim contributed equally to this work.

S. Y. Ryu · D. U. Kim · H. Y. Choi · G. H. Kim · K. S. Chang (✉)
Center for Analytical Instrumentation Development, Korea Basic Science Institute,
169-148 Gwahangno, Yuseong-gu, Daejeon 305-806, Republic of Korea
e-mail: ksc@kbsi.re.kr

J. K. Kim
Biomedical Engineering R&D Center, Asan Institute for Life Sciences,
88 Olympic-ro 43-gil, Songpa-Gu, Seoul 138-736, Republic of Korea

devices, such as a short/near-short circuit, delamination/crack formation, generation of stress gradient areas, and decreases in the effective thermal conductivity, including signal and power integrity problems [1]. Recently, as the development of monolithic integration technology for incorporating microelectronic devices into chips has accelerated, thermal analyses, such as surface temperature profile measurements and localized heat generation detection on the submicron scale, have become essential in the design of reliable electronic components. Therefore, several thermal analysis techniques for avoiding the problems caused by small defects, as listed above, have been developed to investigate the thermal behavior, including the temperature rise, distribution, and gradients in microelectronic devices [2,3]. For example, contact methods such as micro-thermocouples and scanning thermal microscopy (SThM) [4] have been proposed. However, these are invasive methods which could damage the sample. Thus, others have adopted semi-invasive thin-film coating methods such as liquid crystal thermography (LCT) [5] and fluorescence micro-thermography (FMT) [6]. However, for these techniques, pre-sample preparation processes (e.g., thin-film coating, thin layer covering, etc.) are required for the detection procedure. In addition, these processes can affect the thermal conductivity and heat capacity of the sample, resulting in inaccurate thermal analysis for small defect detection.

In comparison with these previous methods, infrared thermography (IRT) [7,8] and thermoreflectance microscopy (TRM) [9–11] have thus emerged as nondestructive and noncontact temperature measurement techniques for microscale and submicron-scale semiconductor devices. An IRT system directly measures the spatial distribution of thermal radiation emitted from the surface of a sample using IR cameras that have a thermal resolution of less than 10~20 mK. Due to its high thermal resolution performance, the IRT technique has been commercially used for measuring thermal distributions and for detecting hotspots on electronic devices. However, the spatial resolution is limited to 3~5 μm , which is not sufficient to detect submicron defects owing to the diffraction limit of mid-infrared (MIR) waves. Thus, a solid immersion lens has been employed to improve the spatial resolution, yet a low signal-to-noise ratio (SNR) can still be a concern [8]. In addition, the low emissivity of metals, which are widely used as electrical contacts in electronic devices, limits the application of IRT [3]. In a TRM system, ultraviolet/visible light and a charge-coupled device (CCD) camera are used to measure the temperature distribution of the target sample. Short wavelength illumination can easily provide the required high spatial resolution in the sub-micrometer range. It has been reported that a CCD-based TRM system with blue illumination can offer thermal and spatial resolutions as small as 10 mK and 250 nm, respectively [9–11].

In this work, we describe the procedure for the quantitative temperature measurement of hotspots generated by defects on a polysilicon microresistor in the TRM system. To confirm the accuracy of the quantitative temperature measurement and small defect isolation, the temperature at the submicron defect in each thermal image obtained by the TRM and IRT systems was directly compared. The good agreement of the temperature and defect location between the two thermal images shows the potential of the TRM system for semiconductor device thermal analysis with good defect detection and quantitative temperature measurement.

2 Experimental Apparatus and Procedures

2.1 Thermoreflectance Microscopy (TRM) System

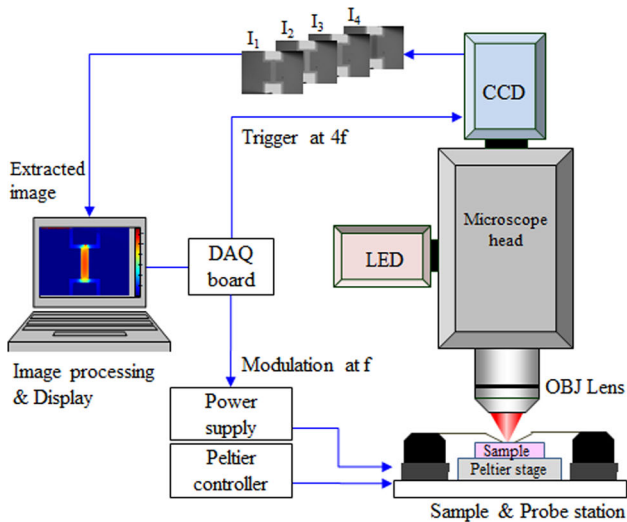
The TRM system provides a thermal imaging technique for measuring the temperature-dependent variation in the reflectivity (R) of a semiconductor device surface. When a temperature variation is generated, the complex dielectric function of the semiconductor varies because of the energy-gap shift due to thermal expansion and electron–phonon interaction [12]. This variation of the complex dielectric function results in variation of the reflectivity of the surface material [13]. Thus, reflectivity variations at the device surface are created by temperature variations. TRM exploits the linear relation between the relative reflectivity variation ($\Delta R/R$) and the temperature variation (ΔT) of the material undergoing thermal analysis [10]:

$$\frac{\Delta R}{R} = \left(\frac{1}{R} \frac{\partial R}{\partial T} \right) \Delta T = \kappa \Delta T, \quad (1)$$

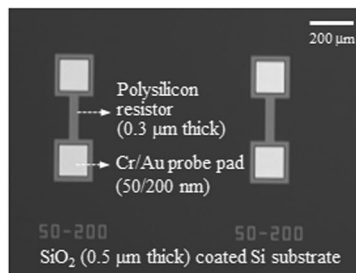
where R and T are the reflectivity and temperature on the sample surface, respectively, and κ is the thermoreflectance calibration coefficient, which depends on the sample material, wavelength of the illuminating light, and angle of incidence. The temperature variation can be obtained by measuring the reflectivity variation (ΔR) with a known κ value.

Figure 1a shows a schematic of the developed TRM system, which is composed of a visible light illuminator, a CCD camera, and a microscope head including an objective lens. A red LED (peak wavelength: 636 nm, MCEP-CR8, Schott Moritex) that induces a large thermoreflectance coefficient on a polysilicon material was used as the illuminator. A 14-bit CCD camera (pco.1600, PCO AG), which has a resolution of 800×600 (2×2 binning) and a 40 Hz maximum frame rate, was employed as the detector. The LED and CCD camera were attached to a conventional microscope head (PSM-1000, Motic). A $20\times$ (0.42 NA, M Plan Apo, Mitutoyo) and a $100\times$ (0.5 NA, M Plan Apo NIR, Mitutoyo) objective lens were utilized to focus the light source onto the sample and to collect the reflected light from the sample. At the sample stage, a probe station was used to apply a voltage bias to the electronic device, and a Peltier element and a resistive temperature detector (RTD) were employed for feedback temperature control of the devices. The trigger and bias modulation signals for lock-in detection were supplied by output signals from the data acquisition (DAQ) board (NI PCIe-6353, National Instruments). For the $100\times$ objective lens (0.5 NA) and the red LED (635.9 nm), we experimentally obtained the thermal and spatial resolution of ~ 13 mK and 670 nm from the thermoreflectance image after 50 000 iterations.

Polysilicon micro-resistors were prepared as test samples, as shown in Fig. 1b. The stripe-patterned micro-resistors were $50 \mu\text{m}$ wide and $200 \mu\text{m}$ long, and the measured resistance was 350Ω .



(a)



(b)

Fig. 1 (a) Schematic of the TRM system for quantitative thermal imaging and (b) a picture of the polysilicon micro-resistors deposited on a SiO_2 -coated Si substrate

2.2 Calibration Process for the Quantitative Temperature Measurement

2.2.1 Determination of the κ Value

In order to obtain the quantitative temperature distribution of a sample surface, the κ value determination and the thermoreflectance image ($\Delta R/R$) acquisition are required. We first determined the κ value. Generally, the κ value is very small (on the order of 10^{-3} to 10^{-5}) and strongly depends on the material, layer structure, and illumination wavelength [8]. As shown in Eq. 1, the κ value can be determined by measuring the relative reflectivity variation as a function of the temperature variation.

During the experiment for κ value determination, the temperature of the sample was maintained by the Peltier stage and the RTD. The process of deriving the κ value is as follows. First, the Peltier stage was set to 20 °C. Next, the reflectivity was measured at best focus. The reflectivity measurement for the homogeneous region of interest on the sample was repeated five times at each set temperature for accuracy and precision.

The set temperature was gradually increased from 20 °C to 60 °C in increments of 2 °C. Then, the relative reflectivity variation and the temperature variation were recorded. Finally, the slope (κ) between the averaged relative reflectivity variation and temperature variation was calculated via linear fitting. The obtained thermoreflectance calibration coefficient (κ) of polysilicon was $-1.71 \times 10^{-3} \text{ K}^{-1}$ under illumination by light with $\lambda = 635.9 \text{ nm}$ and a $20\times$ (0.42 NA) objective lens.

2.2.2 Acquisition of the Thermoreflectance Image

The next procedure required for the quantitative temperature measurement is the thermoreflectance image acquisition from the test sample. Due to the very small κ value, the thermoreflectance image acquisition was accompanied by thermal modulation and lock-in detection techniques to achieve a sufficient SNR. In our experiment, while a sinusoidally-modulated voltage is supplied to the sample at a fixed frequency of 10 Hz (f), a series of four different images (I_1 , I_2 , I_3 , and I_4) is acquired by the CCD camera at a triggering frequency of 40 Hz ($4f$) as shown in Fig. 1a. Using the following relation [9], the thermoreflectance image can be extracted from the four images:

$$\left| \frac{\Delta R}{R} \right| = \frac{\pi}{\sqrt{2}} \frac{\sqrt{(I_1 - I_3)^2 + (I_2 - I_4)^2}}{I_1 + I_2 + I_3 + I_4}. \quad (2)$$

Finally, the temperature variation of the extracted thermoreflectance image was obtained by calibration with the measured κ value.

3 Results and Discussion

Based on the performance of our TRM system, the linear temperature dependence of a polysilicon micro-resistor and the temperature changes in its defect regions have been quantitatively investigated at varying input powers of the devices. Next, the results described in Sect. 2 were compared with results produced with the IRT system as follows, to confirm the ability of the TRM system to provide a quantitative temperature measurement.

A polysilicon micro-resistor which has $50 \mu\text{m}$ width and $200 \mu\text{m}$ length was prepared as a test sample for both the TRM and IRT measurements. In the TRM measurements, a red LED (635.9 nm) and a $20\times$ objective lens (0.42 NA) were used to acquire the thermoreflectance image, and then the temperature variations for the polysilicon resistor region were mapped by applying the measured thermoreflectance coefficient value ($\kappa = -1.71 \times 10^{-3} \text{ K}^{-1}$). Consequently, the true temperature map of the resistor can be obtained by adding the background temperature for each element to the previously mapped temperature variations. The IRT system was simply constructed with an infrared camera (FLIR SC5000, FLIR Systems, Inc.) and the same sample stage setup that was used for the TRM system, including the probe station and the Peltier stage. The IR camera has a 640×512 pixel InSb detector and operates at wavelengths of about $3 \mu\text{m}$ to $5 \mu\text{m}$ with a $5\times$ close-up lens (FLIR Systems, Inc.). The true temperature measurements were performed using the method proposed in

our previous work [15]. Thermal images of the polysilicon micro-resistor in both the TRM and IRT systems were obtained for a range of bias voltages from 0 V to 16 V with increments of 2 V. During both measurements, the background temperature of the micro-resistor was set to 25 °C.

Figure 2a–c shows the quantitatively measured temperature maps of the polysilicon micro-resistor from the TRM system at bias voltages of 8 V, 12 V, and 16 V, respectively. Figure 2d–f presents the corresponding temperature maps of the same polysilicon micro-resistor measured using the IRT system in the same bias conditions. The average temperatures over a $16\ \mu\text{m} \times 165\ \mu\text{m}$ region in the middle of the resistor were obtained in both the TRM and IRT measurements for quantitative comparison of their temperature measuring abilities. As shown in Fig. 2g, the average temperatures

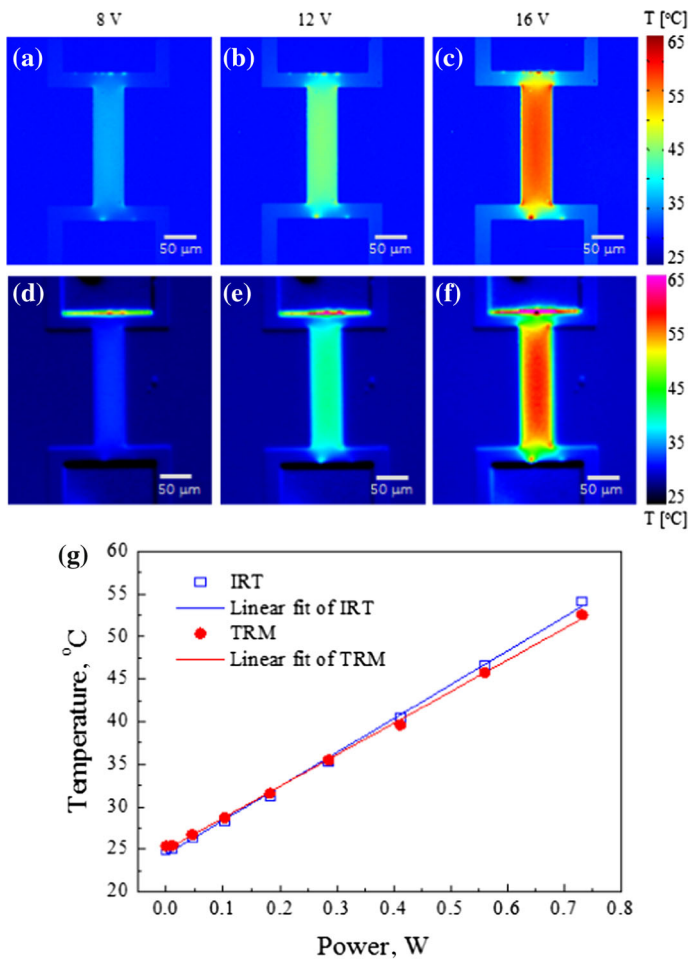


Fig. 2 Temperature maps of a polysilicon micro-resistor measured by the TRM system and IRT system at bias voltages of (a, d) 8 V, (b, e) 12 V, and (c, f) 16 V, respectively. (g) The average temperature of the middle section of the polysilicon micro-resistor

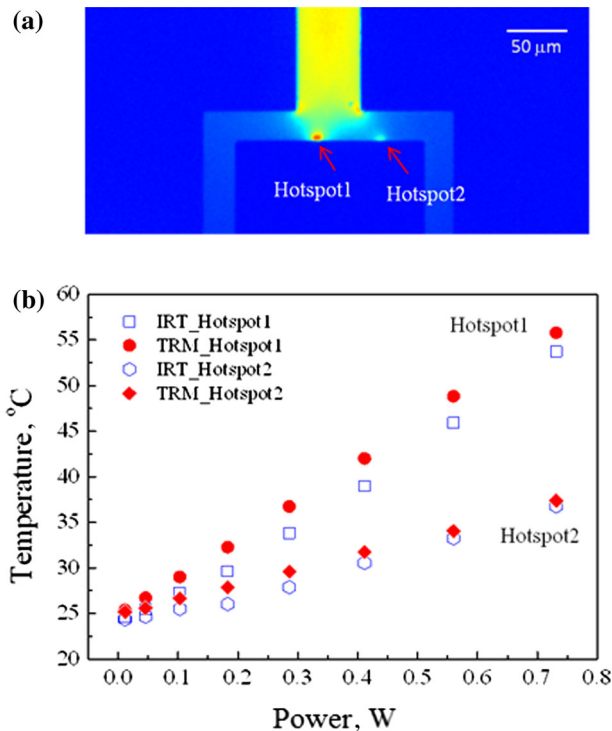


Fig. 3 (a) A temperature map of a part of the polysilicon resistor measured by the TRM system with a bias voltage of 14 V and (b) peak temperatures of the hotspots (arrows) at various bias voltages

linearly increased with slopes of $\sim 38 \text{ }^\circ\text{C} \cdot \text{W}^{-1}$ in both the TRM and IRT measurements. Even though there is a small discrepancy, the temperatures measured by the two different systems are in good agreement with each other. However, the TRM system provides a clearer thermal distribution image than the IRT system due to its high spatial resolution. As seen by comparing Fig. 2c and f, hotspot positions near metal contacts were clearly and individually distinguished in the TRM measurements.

The temperature for localized heat generation such as a hotspot was also compared. Figure 3a shows a part of the temperature map of the polysilicon resistor, which was obtained using the TRM system with a bias voltage of 14 V. As indicated by the arrows, two hotspots were observed at the interface between the polysilicon resistor and the metal contacts. The temperatures of the two different hotspots increased as a function of the applied input power not only in IRT measurements but also in TRM measurements, as shown in Fig. 3b. Each experimental result for the hotspot shows good agreement as well.

To investigate the origin of the hotspots, we observed the hotspots and their nearby regions on the polysilicon resistor in three ways, using a conventional optical microscope image, a TRM image, and a scanning electron microscope (SEM) image. For all measurements, a polysilicon micro-resistor which has $10 \text{ } \mu\text{m}$ width and $200 \text{ } \mu\text{m}$ length was prepared. The conventional optical microscope image, the TRM image,

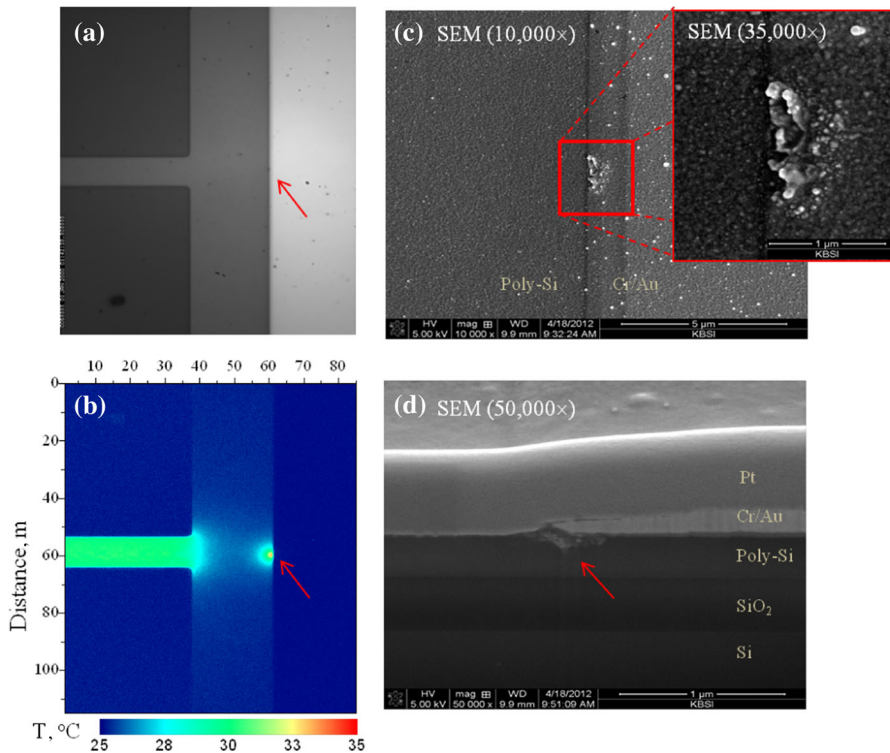


Fig. 4 (a) Conventional microscope image and (b) TRM image around the hotspot region on a polysilicon micro-resistor. (c) SEM images (10 000 \times and 35 000 \times) and (d) cross-sectional SEM image (50 000 \times) of the hotspot region. The sample sizes of (a) and (b) are equal

and SEM images are shown in Fig. 4a, b and c, d, respectively. In the TRM image, the small hotspot region that is barely detectable in the conventional microscope image is clearly distinguished. As shown by the SEM images, we can confirm that a defect of less than 1 μm exists at the location indicated by the arrow. Therefore, we expect that a TRM system can precisely identify the locations of sub-micron scale defects in microelectronic devices by measuring the surface-temperature map.

4 Conclusion

We have demonstrated the capability of the TRM system for quantitative surface temperature measurement and small defect isolation of microelectronic devices. Quantitative temperature measurement of polysilicon microresistors was achieved by not only employing a lock-in detection technique for maximizing the SNR, but also calibrating the thermorefectance image with the experimentally obtained κ value. The linear temperature dependence of hotspots caused by submicron defects was quantitatively measured under varying input powers to verify the quantitative temperature measuring ability of the TRM system by comparison with an IRT system. In the quan-

titative thermal image analysis of the test device, submicron defects could be clearly distinguished and individually isolated. We confirmed both the presence and size of a small defect in the test device by comparing conventional microscope, TRM, and SEM images. Therefore, the proposed TRM system can be a useful noncontact tool for both thermal characterization and submicron-scale defect isolation for a wide range of active microelectronic devices because of its high thermal and spatial resolution.

Acknowledgments This work was supported by the Korea Basic Science Institute Grant D34500.

References

1. Microthermography or Hot Spot Detection. (Silicon Far East Web, 2014). <http://www.siliconfareast.com/hotspotdet.htm>. Accessed 11 April 2014
2. J. Kölzer, E. Oesterschulze, G. Deboy, *Microelectron. Eng.* **31**, 251 (1996)
3. W. Liu, B. Yang, *Sensor Rev.* **27**, 298 (2007)
4. G.B.M. Fiege, V. Feige, J.C.H. Phang, M. Maywald, S. Görlich, L.J. Balk, *Microelectron. Reliab.* **38**, 957 (1998)
5. A. Csendes, V. Székely, M. Rencz, *Microelectron. Eng.* **31**, 281 (1996)
6. D.L. Barton, P. Tangyonyong, *Microelectron. Eng.* **31**, 271 (1996)
7. O. Breitenstein, M. Langenkamp, F. Altmann, D. Katzer, A. Lindner, H. Eggers, *Rev. Sci. Instrum.* **71**, 4155 (2000)
8. O. Breitenstein, F. Altmann, T. Riediger, D. Karg, V. Gottschalk, *Microelectron. Reliab.* **46**, 1508 (2006)
9. P.M. Mayer, D. Lüerßen, R.J. Ram, J.A. Hudgings, *J. Opt. Soc. Am. A* **24**, 1156 (2007)
10. M. Farzaneh, K. Maize, D. Lüerßen, J.A. Summers, P.M. Mayer, P.E. Raad, K.P. Pipe, A. Shakouri, R.J. Ram, J.A. Hudgings, *J. Phys. D: Appl. Phys.* **42**, 143001 (2009)
11. D. Kendig, K. Yazawa, A. Marconnet, M. Asheghi, A. Shakouri, 28th IEEE Semi-Therm Symposium (2012)
12. E. Matatagui, A.G. Thompson, M. Cardona, *Phys. Rev.* **176**, 950 (1968)
13. B. Baltz, in *Semiconductors and Semimetals*, vol. 9, ed. by R.K. Willardson, A.C. Beer (Academic, New York, 1972), pp. 315
14. L.R. De Freitas, E.C. da Silva, A.M. Mansanares, G. Tessier, D. Fournier, *J. Appl. Phys.* **98**, 063508-1-7 (2005)
15. K.S. Chang, S.C. Yang, J.Y. Kim, M.H. Kook, S.Y. Ryu, H.Y. Choi, G.H. Kim, *Sensors* **12**, 4648 (2012)